© 2024. Published by The Company of Biologists Ltd | Development (2024) 151, dev201912. doi:10.1242/dev.201912

RESEARCH ARTICLE

A lissencephaly-associated *BAIAP2* variant causes defects in neuronal migration during brain development

Meng-Han Tsai[1,2,*], Wan-Cian Lin[3,4,*], Shih-Ying Chen[1], Meng-Ying Hsieh[5], Fang-Shin Nian[3,6], Haw-Yuan Cheng[3], Hong-Jun Zhao[3], Shih-Shun Hung[7], Chi-Hsin Hsu[8], Pei-Shan Hou[7], Chien-Yi Tung[8], Mei-Hsuan Lee[6,9] and Jin-Wu Tsai[3,9,10,11,‡]

ABSTRACT

Lissencephaly is a neurodevelopmental disorder characterized by a loss of brain surface convolutions caused by genetic variants that disrupt neuronal migration. However, the genetic origins of the disorder remain unidentified in nearly one-fifth of people with lissencephaly. Using whole-exome sequencing, we identified a *de novo BAIAP2* variant, p.Arg29Trp, in an individual with lissencephaly with a posterior more severe than anterior (P>A) gradient, implicating *BAIAP2* as a potential lissencephaly gene. Spatial transcriptome analysis in the developing mouse cortex revealed that *Baiap2* is expressed in the cortical plate and intermediate zone in an anterior low to posterior high gradient. We next used *in utero* electroporation to explore the effects of the *Baiap2* variant in the developing mouse cortex. We found that *Baiap2* knockdown caused abnormalities in neuronal migration, morphogenesis and differentiation. Expression of the p.Arg29Trp variant failed to rescue the migration defect, suggesting a loss-of-function effect. Mechanistically, the variant interfered with the ability of BAIAP2 to localize to the cell membrane. These results suggest that the functions of BAIAP2 in the cytoskeleton, cell morphogenesis and migration are important for cortical development and for the pathogenesis of lissencephaly in humans.

KEY WORDS: *BAIAP2*, Lissencephaly, Cortical development, Neuronal migration, Epilepsy, Developmental delay, Actin filament, Human, Mouse

INTRODUCTION

Lissencephaly, an archetypal malformation of cortical development in humans, results from neuronal migration defects occurring between the third and the fourth months of gestation. This condition disrupts the proper positioning of cortical neurons, resulting in a lissencephalic cerebrum without normal convolutions of the gyrus and sulcus, along with cortical thickening and potential ventricular enlargement (Barkovich et al., 1991; Dobyns and Truwit, 1995). Individuals with lissencephaly suffer from various neurological deficits, including developmental delay, intellectual disability, motor function impairment, and seizures (Allanson et al., 1998; Dobyns, 2010). Pathogenic variants of more than 30 genes, including *LIS1* (*PAFAH1B1*), *DCX*, *TUBA1A*, *DYNC1H1*, and recently *CEP85L*, account for more than 80% of lissencephaly cases (Tsai et al., 2016, 2020b; Di Donato et al., 2018). Many of these genes encode components of the cytoskeleton, especially microtubules and motor proteins, which play pivotal roles in neuronal migration (Reiner et al., 1993; Lo Nigro et al., 1997; des Portes et al., 1998; Gleeson et al., 1998, 1999; Hong et al., 2000; Kitamura et al., 2002; Tsai et al., 2005, 2020a; Keays et al., 2007; Fry et al., 2014; Jheng et al., 2018; Lin et al., 2022). Despite the advances in understanding the genetics of lissencephaly, the causes of the remaining occurrences of lissencephaly have not been determined.

Here, we identified a *de novo* single nucleotide variant in *BAIAP2* (NM_001144888) from an individual with lissencephaly. BAIAP2 (brain-specific angiogenesis inhibitor 1-associated protein 2), also known as IRSp53 (insulin receptor tyrosine kinase substrate p53), contains an N-terminal IMD (IRSp53 and MIM homology domain), CRIB (Cdc42/Rac interactive binding) motif, SH3 (Src homology 3) domain, and PDZ-B (PDZ-binding) motif (Yamagishi et al., 2004). BAIAP2 functions as a scaffold protein by binding to phospholipids, directing its interacting proteins to the plasma membrane. Additionally, BAIAP2 also possesses the ability to induce membrane deformation, actin bundling, and filopodia formation (Oda et al., 1999; Bockmann et al., 2002; Yamagishi et al., 2004; Suetsugu et al., 2006; Mattila et al., 2007). The potential importance of BAIAP2 in the central nervous system is underscored by its enriched expression in the brain, particularly in the cortex, hippocampus, cerebellum and caudate putamen (Oda et al., 1999; Bockmann et al., 2002). Moreover, BAIAP2 accumulates in the postsynaptic density (PSD) of dendritic spines and colocalizes with postsynaptic proteins Shank and PSD95 (DLG4) (Choi et al., 2005; Scita et al., 2008; Dosemeci et al., 2017). However, *BAIAP2* has not been previously associated with lissencephaly, and its role in cortical development has not been explored.

In this study, we investigated the role of BAIAP2 in the development of the mouse cerebral cortex using *in utero* electroporation (IUE), shedding new light on the role of BAIAP2 in cortical development. We also examined the impact of the newly identified variant on BAIAP2 protein functions and elucidated the

[1]Department of Neurology & Department of Medical Research, Kaohsiung Chang Gung Memorial Hospital, Kaohsiung 833, Taiwan. [2]School of Medicine, Chang Gung University, Taoyuan 333, Taiwan. [3]Institute of Brain Science, College of Medicine, National Yang Ming Chiao Tung University, Taipei 112, Taiwan. [4]Faculty of Medicine, College of Medicine, National Yang Ming Chiao Tung University, Taipei 112, Taiwan. [5]Division of Pediatric Neurology, Department of Pediatrics, Chang Gung Memorial Hospital, Taipei 105, Taiwan. [6]Institute of Clinical Medicine, College of Medicine, National Yang Ming Chiao Tung University, Taipei 112, Taiwan. [7]Institute of Anatomy and Cell Biology, National Yang Ming Chiao Tung University, Taipei 112, Taiwan. [8]Genomics Center for Clinical and Biotechnological Applications, Cancer Progression Research Center, National Yang Ming Chiao Tung University, Taipei 112, Taiwan. [9]Advanced Therapeutics Research Center, National Yang Ming Chiao Tung University, Taipei 112, Taiwan. [10]Brain Research Center, National Yang Ming Chiao Tung University, Taipei 112, Taiwan. [11]Department of Biological Science and Technology, College of Biological Science and Technology, National Yang Ming Chiao Tung University, Hsinchu 300, Taiwan.
*These authors contributed equally to this work

‡Author for correspondence (tsaijw@nycu.edu.tw)

J.-W.T., 0000-0003-0135-759X

Handling Editor: Debra Silver
Received 26 April 2023; Accepted 12 December 2023

DEVELOPMENT

Development (2024) 151, dev201912. doi:10.1242/dev.201912

mechanism by which this variant contributes to the pathogenesis of lissencephaly.

RESULTS

Identification of a *de novo BAIAP2* variant in an individual with lissencephaly

First, we identified a 6-year-old individual with unexplained lissencephaly in Taiwan. Previous genetic testing showed no pathogenic variants in known lissencephaly genes. Clinically, this individual exhibited severe global developmental delay since infancy, characterized by a lack of speech development and poor motor milestone achievement. They also experienced refractory epilepsy with multiple seizure patterns, including focal, myoclonic, tonic, absence and tonic-clonic seizures, and epileptic spasms since infancy. Electroencephalogram results revealed paroxysmal generalized poly-spike and waves. Despite receiving multiple antiseizure medications, ketogenic diet therapy, and vagus nerve stimulation, the individual continued to suffer from frequent seizures. T1-weighted magnetic resonance image (MRI) at the age of 5 years and 5 months revealed severe diffuse loss of cortical convolutions and thickened cortex with posterior regions more severely affected than the anterior regions (P>A gradient), consistent with classical lissencephaly. In addition, the MRI showed reduced white matter, enlarged ventricles with wavy wall configuration, and prominent subcortical strips (Fig. 1A).

Owing to the absence of a family history and the severe phenotype, resembling other lissencephaly cases, we assumed a *de novo* mutation as the most likely inheritance model. Using trio whole-exome sequencing, we identified two *de novo* variants after filtering, including one non-frameshift and one missense variant (Table S1). The heterozygous missense variant, c.C85T (p.Arg29Trp), in *BAIAP2* (NM_001144888; Fig. 1B,C) was validated by Sanger sequencing. Predictive algorithms, including SIFT, PolyPhen and MutationTaster2, collectively suggested that this variant was damaging/disease-causing, with a combined annotation dependent depletion (CADD) score of 34. Additionally, *BAIAP2* was prioritized as the top candidate gene due to its functional relevance to the cytoskeleton. Interestingly, the *BAIAP2* p.Arg29Trp variant is located within the N-terminal IMD of the BAIAP2 protein, which interacts with small GTPases and the actin cytoskeleton to regulate membrane dynamics (Fig. 1C). However, *BAIAP2* has not been reported as a causative gene in lissencephaly, and its functional roles in cortical development remain unexplored.

Baiap2 is expressed in an anterior low to posterior high gradient in the developing cortex

To investigate the role of BAIAP2 in cortical development, we first examined the expression of BAIAP2 protein in the mouse cortex at various developmental stages, from embryonic (E) day 13.5 to postnatal (P) day 30. Western blotting of protein lysates from mouse cortices showed that BAIAP2 expression gradually increased with age from E13.5 to P30 (Fig. 1D), suggesting a potential role for BAIAP2 throughout these developmental stages. Additionally, we observed a protein of lower molecular weight, corresponding to a C-terminal splicing short isoform (Scita et al., 2008), which was present at E13.5 and exhibited a gradual reduction after E14.5, suggesting its participation in earlier developmental stages.

Given the observed anterior low to posterior high gradient of cortical malformation observed in the human MRI scans, we examined *Baiap2* expression patterns in the developing mouse cortex using spatial gene expression profiling (Chen et al., 2022). Four equally spaced sagittal sections from an E15.5 mouse brain were mounted on a specialized slide, on which mRNA was captured and barcoded with spatial information. The expression profiles for each captured area were obtained through sequencing of a cDNA library. Based on the similarity of expression profiles, all captured areas were grouped into 12 clusters, among which cortical plate (CP), intermediate zone (IZ) and ventricular zone (VZ) were clearly separated (Fig. 2A). We found that *Baiap2* was specifically expressed in the CP and IZ (Fig. 2A,B). Interestingly, *Baiap2* expression exhibited a gradient pattern from anterior-low to posterior-high (Fig. 2A,C).

To confirm the gradient expression pattern, we performed *in situ* hybridization analysis of the developing mouse cortex at E15.5. The results showed that the RNA expression of *Baiap2* was enriched in the lower cortical plate region, showing a posterior-high to anterior-low pattern (Fig. 2D), consistent with the findings from spatial gene expression profiling (Fig. 2A-C). Furthermore, immunofluorescence staining of BAIAP2 in the developing mouse cortex was performed to confirm the expression of BAIAP2 protein. We found that the BAIAP2 signal was notably higher in the posterior part of the CP compared with the anterior end (Fig. 2E), indicating an anterior-low to posterior-high gradient of BAIAP2 expression in the developing cortex.

To corroborate these findings in the human fetal forebrain, we performed *in silico* analysis of the future prefrontal cortex and visual cortex using a human gestation week (GW) 20 cortical single-cell RNA sequencing dataset (Bhaduri et al., 2021). The results showed that BAIAP2 was enriched in the future visual area, corresponding to the posterior region of the forebrain (Fig. 2F). Collectively, these results reveal a strong correlation between BAIAP2 expression and the severity of the cortical malformation.

Baiap2 knockdown impairs neuronal migration and morphogenesis

To investigate the impact of BAIAP2 loss of function on cortical development, we used IUE of short-hairpin RNA (shRNA) to knock down *Baiap2* expression in the developing cortex of mouse embryos (Lu et al., 2018; Chen et al., 2019). We first evaluated the knockdown efficiency of shRNA constructs (sh*Baiap2* #54, #57, #312 and #498) by transfecting them into Neuro-2a (N2a) cells. Western blot analysis of cell lysates showed that sh*Baiap2* #54 and #498 reduced BAIAP2 expression most effectively compared with control cells transfected with scrambled shRNA (shCtrl) (Fig. 3A). These shRNA constructs, along with green fluorescent protein (GFP) cDNA, were then electroporated into mouse cortex at E14.5 and the distributions of GFP^+ cells were observed in brain sections at E18.5. In control brains electroporated with shCtrl, most of the GFP^+ cells migrated successfully to the CP (68.7±1.5%; mean±s.e.m.). In contrast, brains electroporated with sh*Baiap2* #54 and #498 displayed fewer GFP^+ cells in the CP (sh*Baiap2* #54: 34.1±4.3%, $P<0.001$; sh*Baiap2* #498: 29.6±5.9%; $P<0.01$; one-way ANOVA with post-hoc Tukey's test), with a majority of cells delayed in the IZ (sh*Baiap2* #54: 35.7±2.6%; sh*Baiap2* #498: 50.3±3.7%; versus shCtrl: 16.8±1.4%; $P<0.001$; one-way ANOVA with post-hoc Tukey's test; Fig. 3B).

In addition to migration defects, *Baiap2* knockdown in the developing cortex also led to abnormal cell morphology in the IZ. In control cortices, most GFP^+ cells electroporated at E14.5 had transitioned into a bipolar state by E18.5, consistent with previous findings in the developing cortex (Kriegstein and Noctor, 2004; Lu et al., 2018). In brains electroporated with sh*Baiap2*, an increased number of multipolar cells were found in the IZ (sh*Baiap2* #54: 41.6 ±3.2%; sh*Baiap2* #498: 51.3±1.0% versus shCtrl: 18.7±3.3%;

Development (2024) 151, dev201912. doi:10.1242/dev.201912

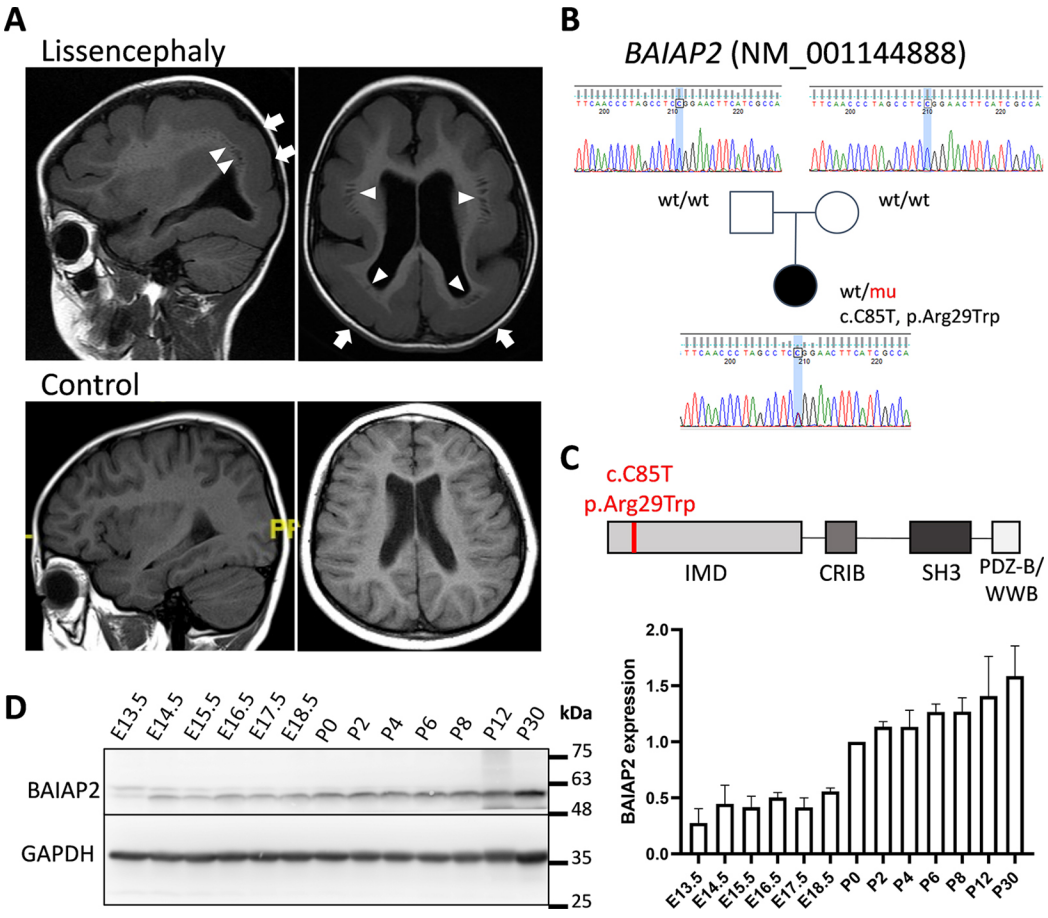

Fig. 1. Severe lissencephaly in an individual with a *BAIAP2* variant and expression of BAIAP2 during brain development in mice. (A) Top: T1-weighted MR brain images revealed diffuse classical thick agyria-pachygyria, which is more severe in the posterior regions (arrows). Prominent subcortical T1 low signal strips within the white matter over bilateral parietal and frontal regions are noted (arrowheads). Bottom: Brain MRI of an age-matched control individual. (B) Pedigree of the individual with lissencephaly caused by a *de novo BAIAP2* missense variant. c.C85T (p.Arg29Trp) variant was confirmed by Sanger sequencing. (C) Schematic of BAIAP2 protein domains and with location of the p.Arg29Trp variant marked. BAIAP2 contains an IMD, a CRIB motif, an SH3 domain and a WWB/PDZ-B motif. The variant p.Arg29Trp is located in the IMD. (D) Western blot of BAIAP2 protein in the cerebral cortex of ICR mice from E13.5 to P30. BAIAP2 was expressed at all stages examined and gradually increased during this period. The bar graph shows relative BAIAP2 expression after normalization to its expression at P0. Error bars represent s.e.m. *n*=3 independent experiments.

P<0.01; one-way ANOVA with post-hoc Tukey's test; Fig. 3C). These results indicate the importance of BAIAP2 in regulating both neuronal migration and morphogenesis during cortical development.

To investigate whether the effects of *Baiap2* knockdown on neuronal migration and morphogenesis were a consequence of earlier neurogenesis events, we examined the expression of progenitor cell markers Pax6 and Tbr2 (Eomes) 2 days after IUE (Fig. S1). We found that *Baiap2* knockdown did not significantly alter the proportion of Pax6$^+$ and Tbr2$^+$ cells among the electroporated GFP$^+$ cells. This finding is consistent with the low expression pattern of *Baiap2* in the VZ/subventricular zone (SVZ) region and suggests that BAIAP2 mainly functions in postmitotic neurons.

Baiap2 knockdown altered neuronal fate

To examine further the effects of *Baiap2* knockdown on cell differentiation, brain slices were collected at P7 after IUE at E14.5 (Fig. 4). In control brains electroporated with shCtrl, nearly all GFP$^+$ cells (97.7±1.3%) reached layer II/III of the cortex by P7. However, in brains electroporated with sh*Baiap2* #498, a subset of cells (29.85 ±8.14%) remained localized in the white matter (WM) (Fig. S2). Intriguingly, among the cells that had migrated to the cortex, they appeared to be positioned more superficially within layer II/III (Fig. S2A,C).

To investigate the fate of *Baiap2* knockdown cells, particularly those arrested in the WM, we performed immunofluorescence staining using the neuronal marker NeuN (Rbfox3) (Fig. 4A) and the layer II/III (and V) marker Brn2 (Pou3f2) (Fig. 4B) (Chang et al., 2019). In control brains electroporated with shCtrl, the majority of GFP$^+$ cells expressed NeuN (95.9±1.4%) and Brn2 (67.7±3.1%). In brains electroporated with sh*Baiap2*, most of the cells in layer II/III expressed NeuN (97.2±0.5%) and Brn2 (66.9±1.3%), resembling the expression pattern in control brains. Interestingly, among the *Baiap2* knockdown cells arrested in the WM, we observed a dramatic decrease in the percentage of NeuN$^+$ (35.7±6.1%) and Brn2$^+$ (36.4±8.1%) cells (Fig. 4). To examine whether these cells adopted astrocyte or oligodendrocyte fates, brain slices were stained with glial fibrillary acidic protein (GFAP) and Olig2 antibodies (Fig. S3). Virtually none of the electroporated cells expressed these markers, suggesting that they did not undergo a change in cell fate to become glial cells. These results suggested that *Baiap2* knockdown may arrest some cells in the WM with a yet-to-be-determined cell fate.

Development (2024) 151, dev201912. doi:10.1242/dev.201912

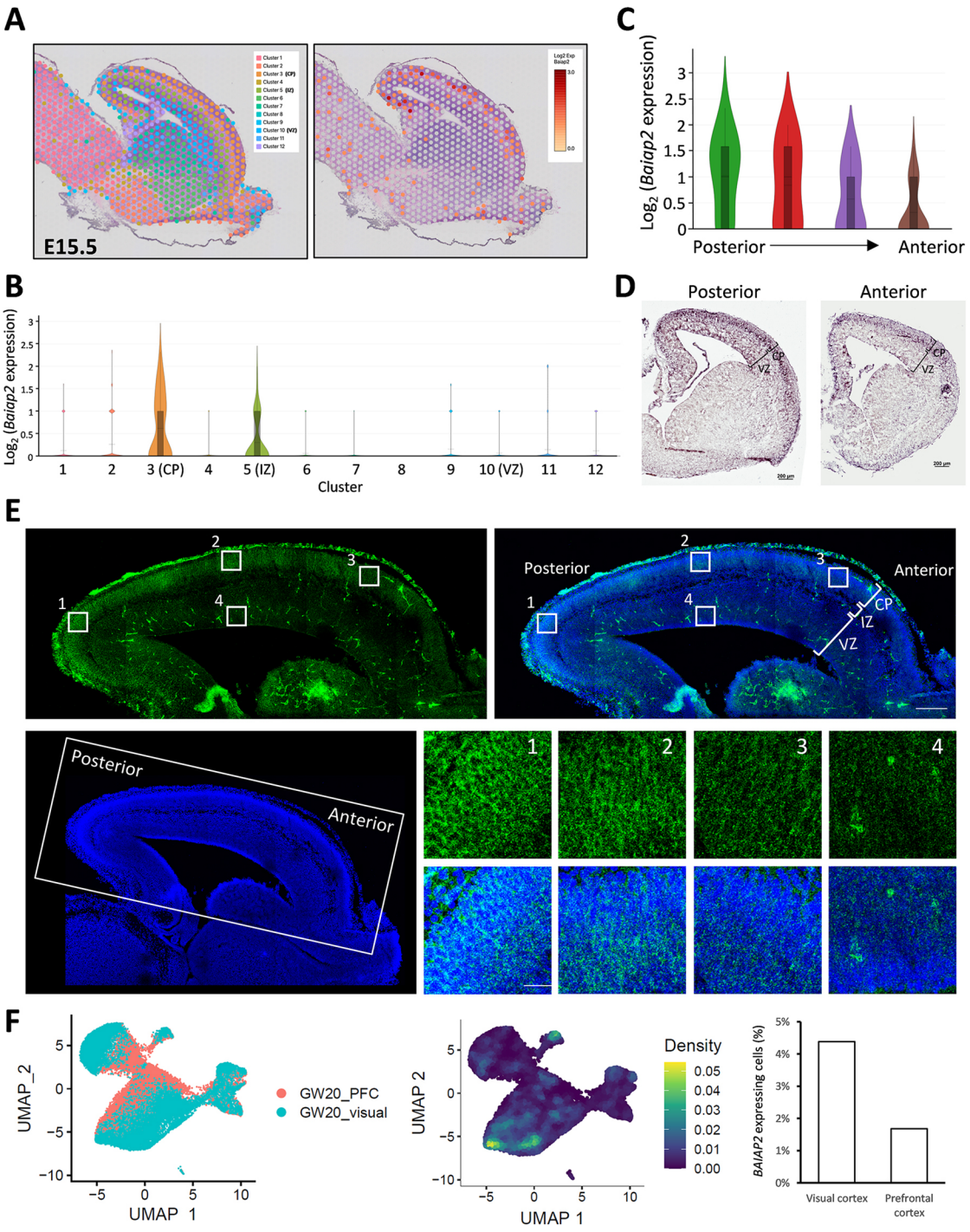

Fig. 2. Spatial distribution of BAIAP2 expression in the developing cerebral cortex. (A) Spatial distribution of *Baiap2* expression in the dorsal telencephalon of the mouse brain at E15.5. Each capture dot was grouped into 12 clusters based on their expression profiles (left). Groups 3, 5 and 10 clearly correspond to the CP, IZ and VZ, respectively. The color scale represents the log-normalization of the unique molecular identifier (UMI) count (right). (B) Violin plot illustrating the log-normalized expression of *Baiap2* in each cluster. *Baiap2* was expressed highly in the CP (cluster 3) and IZ (cluster 5), but not in VZ (cluster 10) or other clusters. (C) Violin plot showing the expression of *Baiap2* from anterior to posterior parts of the cortex. The capture dots corresponding to the dorsal telencephalon were separated into four groups along the anterior-posterior axis. *Baiap2* was expressed at higher levels in the posterior part than in the anterior part. (D) *In situ* hybridization of *Baiap2* in coronal sections of embryonic mouse brains at E15.5. *Baiap2* mRNA is expressed at a higher level in the CP of the posterior section compared with the anterior section. (E) BAIAP2 (green) protein expression in a sagittal section of E15.5 mouse brain using immunofluorescence staining. Endogenous BAIAP2 expression exhibited a high-to-low gradient along the posterior to the anterior axis (from boxes 1 to 3). Enlarged images from the boxes show that BAIAP2 exhibited higher expression levels in the posterior region (1) compared with the anterior region (3). BAIAP2 expression in the VZ was very low (4). Brain slices were counterstained with DAPI (blue) to visualize cell nuclei. (F) UMAP plot of single-cell RNA sequencing of human visual and prefrontal cortices (PFC) at GW20. The heat map of *BAIAP2* expression shows a higher level in the visual cortex than in the PFC. The bar graph shows the percentage of cells expressing *BAIAP2* in each cortical region. Scale bars: 200 µm (D,E top panels); 25 µm (E1-E4).

Development (2024) 151, dev201912. doi:10.1242/dev.201912

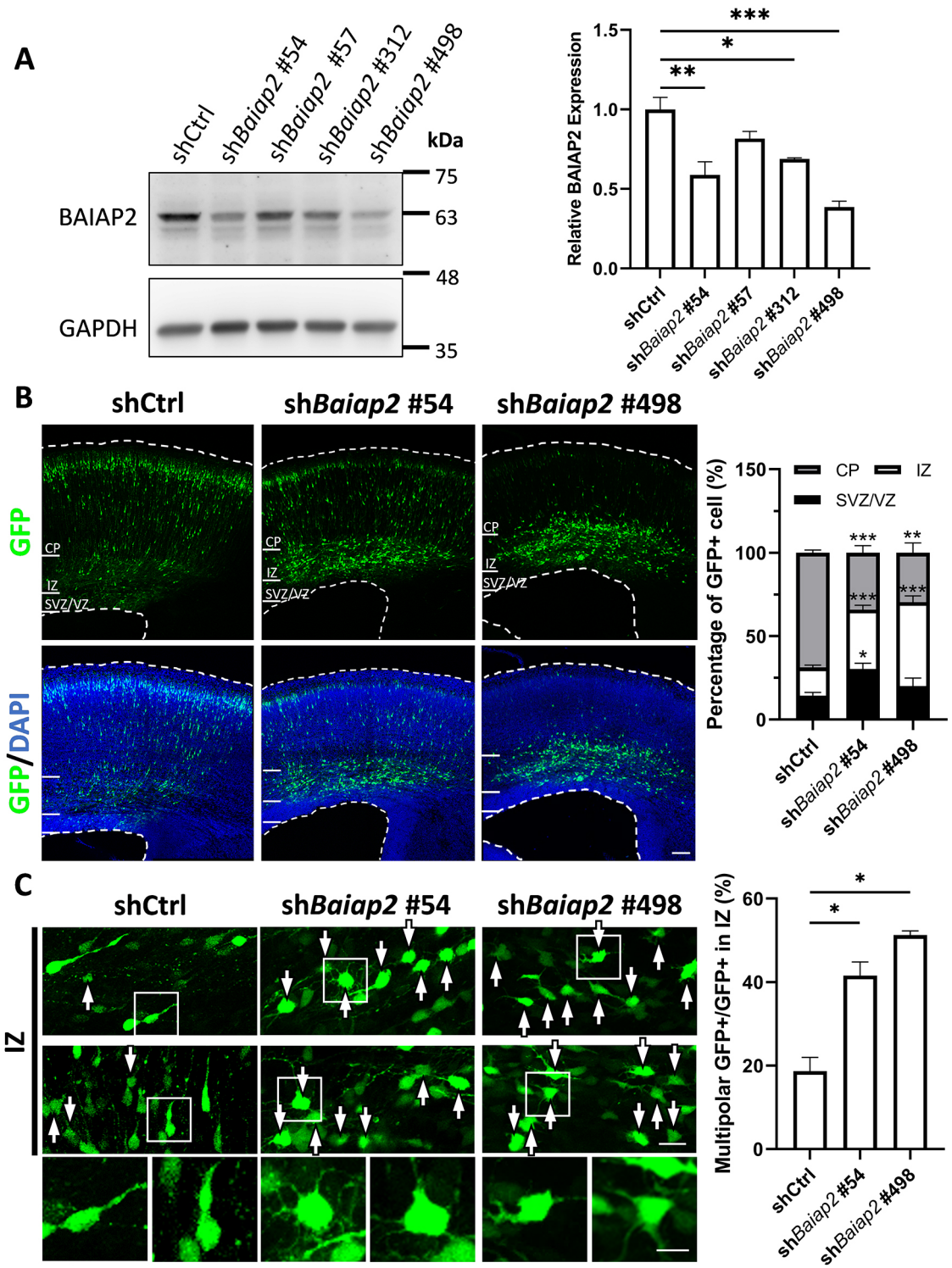

Fig. 3. Cell distribution and morphology after *Baiap2* knockdown in the developing mouse cortex. (A) BAIAP2 expression determined by western blotting in N2a cells transfected with control or *Baiap2* shRNAs. *Baiap2* shRNAs #54 and #498 exhibited the best knockdown efficiency in transfected cells. The bar graph shows BAIAP2 expression normalized to the control. Error bars represent s.e.m. **P*<0.05, ***P*<0.01, ****P*<0.001 (one-way ANOVA with post-hoc Tukey's test); *n*=4. (B) Distribution of electroporated cells in the developing cortex 4 days after IUE of shCtrl and sh*Baiap2*. Most GFP$^+$ cells (green) in brains electroporated with shCtrl had migrated to the CP, whereas most GFP+ cells in brains electroporated with sh*Baiap2* #54 and #498 were distributed in the IZ. Brain slices were counterstained with DAPI (blue) to show cell nuclei. The stacked bar graph shows the percentages of GFP$^+$ cells distributed in the CP, IZ and SVZ/VZ. Error bars represent s.e.m. **P*<0.05, ***P*<0.01, ****P*<0.001 (one-way ANOVA with post-hoc Tukey's test); *n*≥5. (C) Morphology of GFP$^+$ cells in the IZ. Most GFP$^+$ cells in control brains electroporated with shCtrl showed bipolar morphology. Most *Baiap2* knockdown cells exhibited multipolar morphology (arrows). Bipolar cells in the control brain and multipolar cells in the shRNA-electroporated brain are shown at higher magnification in the insets beneath. The bar graph shows the percentage of multipolar cells in the IZ. Error bars represent s.e.m. **P*<0.05 (one-way ANOVA with post-hoc Tukey's test); *n*≥3. Scale bars: 100 µm (B); 20 µm (C, main panels); 10 µm (C, insets).

Development (2024) 151, dev201912. doi:10.1242/dev.201912

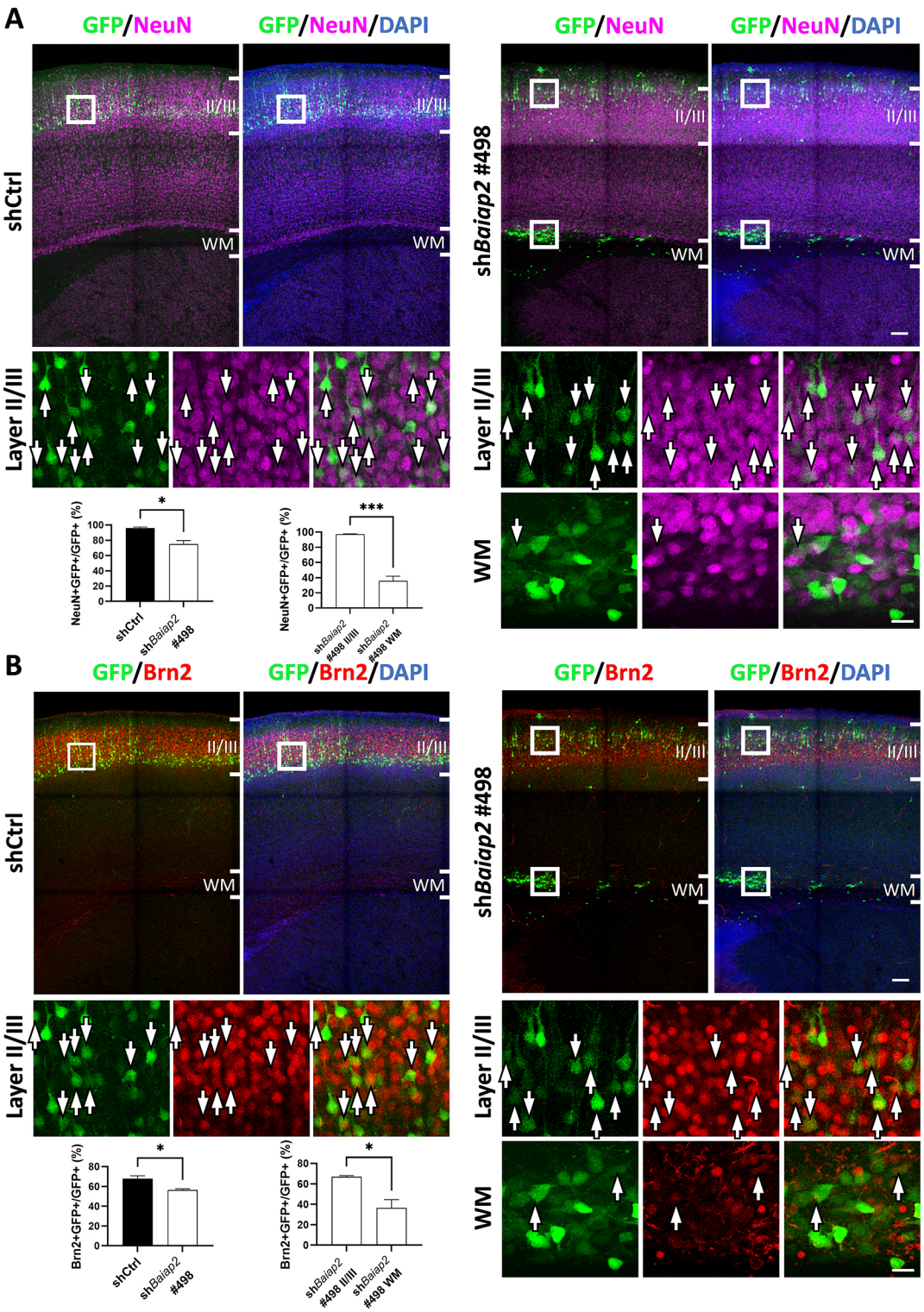

Fig. 4. Neuronal marker expression after *Baiap2* knockdown in postnatal mouse cortex. (A) Immunostaining of NeuN in P7 cortices electroporated with sh*Baiap2* or shCtrl at E14.5. Most GFP$^+$ cells in brains electroporated with shCtrl, and in layer II/III of brains electroporated with sh*Baiap2* #498 were NeuN$^+$ (magenta). In contrast, few GFP$^+$ cells distributed in the WM of brains electroporated with sh*Baiap2* expressed NeuN. Brain slices were counterstained with DAPI (blue) to show cell nuclei. Arrows indicate GFP$^+$ cells with NeuN expression. Bar graphs show the percentage of NeuN and GFP double-positive cells among GFP$^+$ cells in different groups and brain regions. Error bars represent s.e.m. *P<0.05, ***P<0.001 (one-way ANOVA with post-hoc Tukey's test); n=3. (B) Immunostaining of Brn2 in P7 cortex of electroporated brains. Most GFP$^+$ cells in control brains electroporated with shCtrl, as well as in layer II/III of brains electroporated with sh*Baiap2* #498, were Brn2$^+$ (red). In contrast, only a few GFP$^+$ cells distributed in the WM of brains electroporated with sh*Baiap2* expressed Brn2. Brain slices were counterstained with DAPI (blue) to show cell nuclei. Arrows indicate GFP$^+$ cells with NeuN expression. Bar graphs show the percentage of Brn2 and GFP double-positive cells among GFP$^+$ cells in different groups and brain regions. Error bars represent s.e.m. *P<0.05 (one-way ANOVA with post-hoc Tukey's test); n=3. Scale bars: 100 µm (upper panels); 20 µm (lower panels).

Development (2024) 151, dev201912. doi:10.1242/dev.201912

The p.Arg29Trp variant failed to rescue neuronal migration delay

To examine the effects of the lissencephaly-associated *BAIAP2* variant on cortical development, we introduced cDNA expressing the p.Arg29Trp variant into developing mouse brains by IUE at E14.5 (Fig. S4). In control brains electroporated with the empty vector pCAGIG, most of the GFP^+ cells (75.6±3.1%) migrated to the outer CP by E18.5. Brains electroporated with wild-type (WT) *BAIAP2* showed a similar cell distribution pattern across the anterior, medial and posterior regions of the cortex, despite differences in the endogenous BAIAP2 expression along the anterior-posterior axis (Fig. S4). Interestingly, overexpression of the p.Arg29Trp variant did not alter the distribution of cells in the cortex, suggesting that the p.Arg29Trp may not exert dominant-negative effects on cortical development. The expression of BAIAP2 was further validated through immunostaining of the HA tag (Fig. S5).

Given that overexpression of the p.Arg29Trp variant did not cause neuronal migration delay, we next examined its ability to rescue the migration delay caused by sh*Baiap2*. cDNAs expressing WT BAIAP2 and p.Arg29Trp were each co-electroporated with sh*Baiap2* into the developing mouse brains at E14.5 by IUE. The expression levels of WT BAIAP2 and p.Arg29Trp were not diminished when co-transfected with sh*Baiap2* in cells (Fig. S6). Most of the GFP^+ cells co-electroporated with sh*Baiap2* and WT *BAIAP2* were able to migrate to the CP (#54: 68.3±0.3%; #498: 59 ±3.5%), indicating that the abnormal cell distribution caused by *Baiap2* knockdown was partially rescued by BAIAP2 expression (Fig. 5). In contrast, in brains co-electroporated with sh*Baiap2* and the p.Arg29Trp variant, the cell distribution was similar to that of brains electroporated with sh*Baiap2* alone (#54: 37%±4.9 % in CP, 54.4%±4.5 % in IZ; #498: 42.5±6.1% in CP, 29.7±9.5% in IZ; Fig. 5). These results suggest that BAIAP2 p.Arg29Trp is more likely to be a loss-of-function variant.

p.Arg29Trp variant does not disrupt BAIAP2 dimerization

Given that the p.Arg29Trp variant was located in the IMD, which mediates the dimerization of BAIAP2, we next tested whether the variant disturbs BAIAP2 dimerization. Flag- and GFP-tagged BAIAP2 were co-transfected into HEK293T cells (Fig. 6) and immunoprecipitated by magnetic beads coated with GFP antibody. We found that there was no significant difference among WT-to-WT, WT-to-p.Arg29Trp, and p.Arg29Trp-to-p.Arg29Trp interactions (Fig. 6B,C), indicating that the BAIAP2 p.Arg29Trp variant maintains the ability to dimerize with both WT BAIAP2 and p.Arg29Trp in cells.

p.Arg29Trp variant reduces BAIAP2 localization to the cell membrane

Previously, BAIAP2 was found to interact with actin filaments and membrane phospholipids, enabling its localization to the cell periphery (Oda et al., 1999; Yamagishi et al., 2004; Suetsugu et al., 2006; Mattila et al., 2007). Therefore, we investigated how the p.Arg29Trp variant affected the subcellular localization of BAIAP2 in relation to actin filaments. GFP-BAIAP2 WT and p.Arg29Trp were each expressed in N2a cells for 24 h and then stained with fluorescently labeled phalloidin to stain actin filaments. We found that WT BAIAP2 and actin filaments were highly localized to the cell periphery (Fig. 7A), which is consistent with previous observations (Oda et al., 1999). In contrast, the p.Arg29Trp variant exhibited a more diffuse distribution in the cytoplasm with less located at the cell periphery (Fig. 7A). To examine the distribution of BAIAP2 in migrating neurons during cortical development, brains electroporated with HA-tagged BAIAP2 or the p.Arg29Trp variant were stained with the HA antibody. Both WT BAIAP2 and the p.Arg29Trp variant were detected in the leading processes and cell soma. However, the resolution did not allow for a clear differentiation between the membrane and cytoplasmic distribution (Fig. S5).

To confirm the altered subcellular distribution of the p.Arg29Trp variant, we separated protein lysates from cells transfected with WT BAIAP2 and p.Arg29Trp into cytoplasmic and membrane fractions (Fig. 7B). We found a significant decrease of the p.Arg29Trp variant in the membrane fraction (0.75±0.03 fold relative to WT; $P<0.001$, unpaired two-tailed *t*-test) and a small but significant increase of p.Arg29Trp in the cytoplasmic fraction (1.16±0.04 fold relative to WT; $P<0.05$, unpaired two-tailed *t*-test). The subtlety in the difference may be attributed to the potential loss of some BAIAP2 protein from the membrane fraction during preparation. Nevertheless, these results indicated that the p.Arg29Trp variant may decrease the ability of BAIAP2 to localize to the cell membrane.

DISCUSSION

In this study, we identified a *de novo* variant p.Arg29Trp in a novel lissencephaly gene, *BAIAP2*. We showed that *Baiap2* was specifically expressed in the IZ and CP in a rostral-low to caudal-high gradient in the brain of mouse embryos. *Baiap2* knockdown in the developing mouse cortex led to defects in neuronal migration, morphogenesis and differentiation, implicating the importance of BAIAP2 in these processes of cortical development. Expression of BAIAP2 p.Arg29Trp failed to rescue the migration defects of neurons, indicating a loss-of-function effect of this variant. We further examined the effects of the p.Arg29Trp variant on BAIAP2 functions and found that BAIAP2 localization to the plasma membrane was decreased. We propose that the p.Arg29Trp missense variant may have a partial loss-of-function effect on BAIAP2 protein and thus impede neuronal migration, which leads to lissencephaly (Fig. 8).

The identification of p.Arg29Trp *BAIAP2* variant in an individual with lissencephaly suggests the participation of BAIAP2 in neuronal migration during cortical development. Indeed, we found that *Baiap2* was specifically expressed in the IZ and CP of the E15.5 mouse cortex (Fig. 2), which contains predominantly migrating and postmitotic neurons. Knockdown of *Baiap2* resulted in neuronal migration delay, and, whereas WT BAIAP2 only partially rescued the phenotype for reasons yet unknown, the p.Arg29Trp variant failed to do so. Although it remains unclear why WT BAIAP2 could not fully rescue the phenotype, one possibility is that BAIAP2 overexpression may affect neural progenitors, where BAIAP2 is not normally expressed. Interestingly, *Baiap2* was expressed in an anterior-low to posterior-high gradient in the developing mouse cortex (Fig. 2), which correlated with the P>A severity of lissencephaly observed in the human MRI scans (Fig. 1A). It is possible that BAIAP2 dysfunction affects the development of the posterior part of the cerebral cortex as a result of its expression pattern. How the expression of different lissencephaly genes affects the patterning of gyral formation remains an intriguing question.

Moreover, we observed morphological changes in delayed cells in embryonic and postnatal stages (Figs 3C and 4). During cortical development, neuronal precursors undergo a transition from the multipolar to the bipolar state before neuronal migration (Kriegstein and Noctor, 2004; Tsai et al., 2005; Chen et al., 2018). These findings suggest that BAIAP2 may function in the transition of cell morphology and interfere with subsequent neuronal migration,

Development (2024) 151, dev201912. doi:10.1242/dev.201912

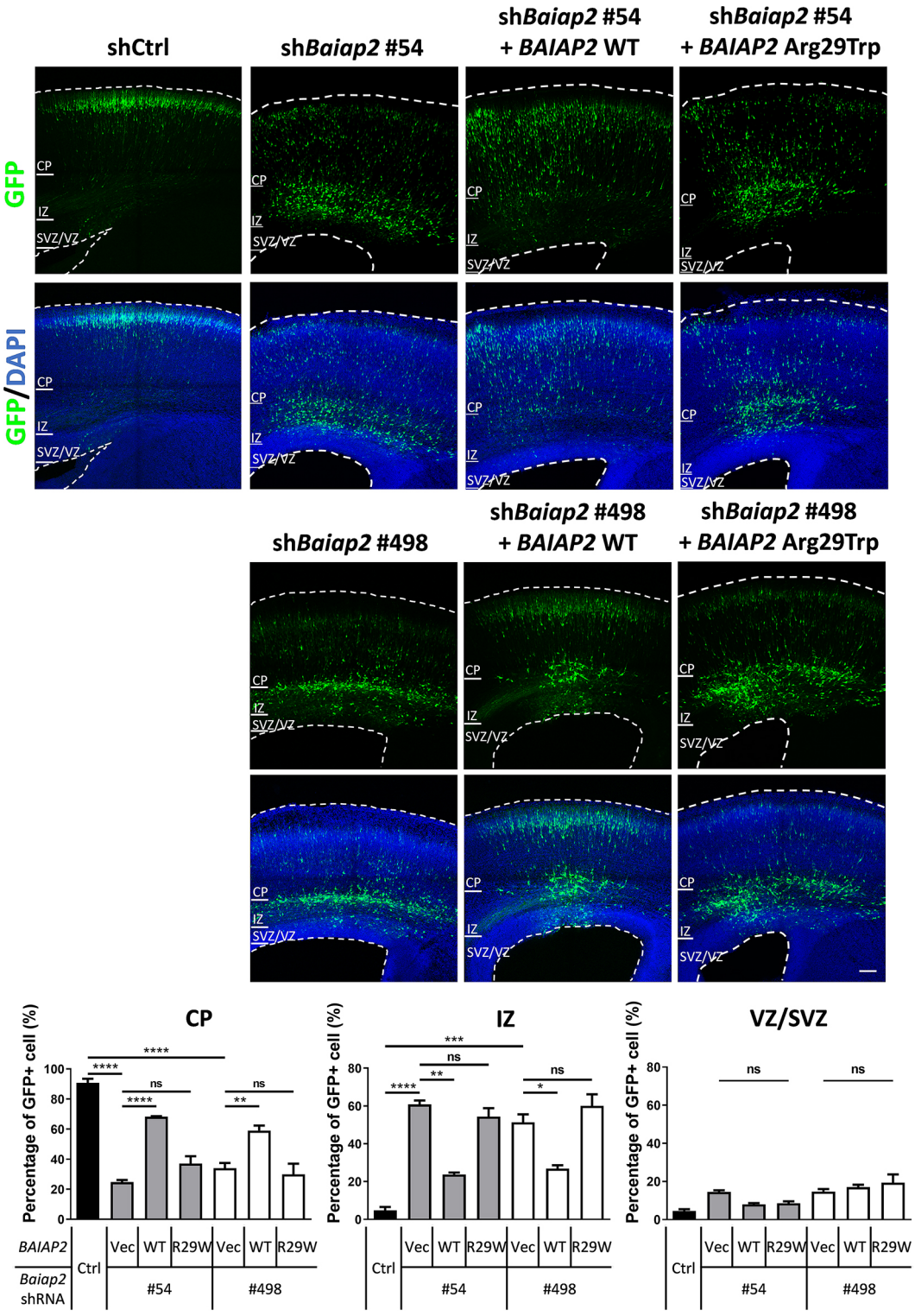

Fig. 5. Cell distribution in developing mouse brains electroporated with sh*Baiap2* and *BAIAP2* cDNA. Cell distribution in the cortex of brains electroporated with sh*Baiap2* #54 or #498 in combination with *BAIAP2* or p.Arg29Trp variant 4 days after IUE. The distribution of GFP$^+$ cells (green) in the IZ indicated that migration was delayed in brains electroporated with sh*Baiap2*. Expression of WT BAIAP2 partially rescued the defect, with more cells reaching the CP. p.Arg29Trp did not significantly change the cell distribution compared with knockdown brains. Brain slices were counterstained with DAPI (blue) to show cell nuclei. Scale bar: 100 µm. The bar graph shows the percentage of GFP$^+$ cells in the CP, IZ and SVZ/VZ. Error bars represent s.e.m. **P*<0.05, ***P*<0.01, ****P*<0.001, *****P*<0.0001 (one-way ANOVA with post-hoc Tukey's test); $n \geq 3$. ns, not significant; R29W, Arg29Trp; Vec, pCAGIG vector.

providing a possible mechanism of BAIAP2 dysfunction in causing lissencephaly. For those cells that had migrated to the cortex at P7, the cell soma appeared to reside more superficially in layer II/III. This observation may indicate a potential role of BAIAP2 in terminal somal translocation, as suggested in studies of neurons deficient of other actin-related proteins (Santana and Marzolo,

Development (2024) 151, dev201912. doi:10.1242/dev.201912

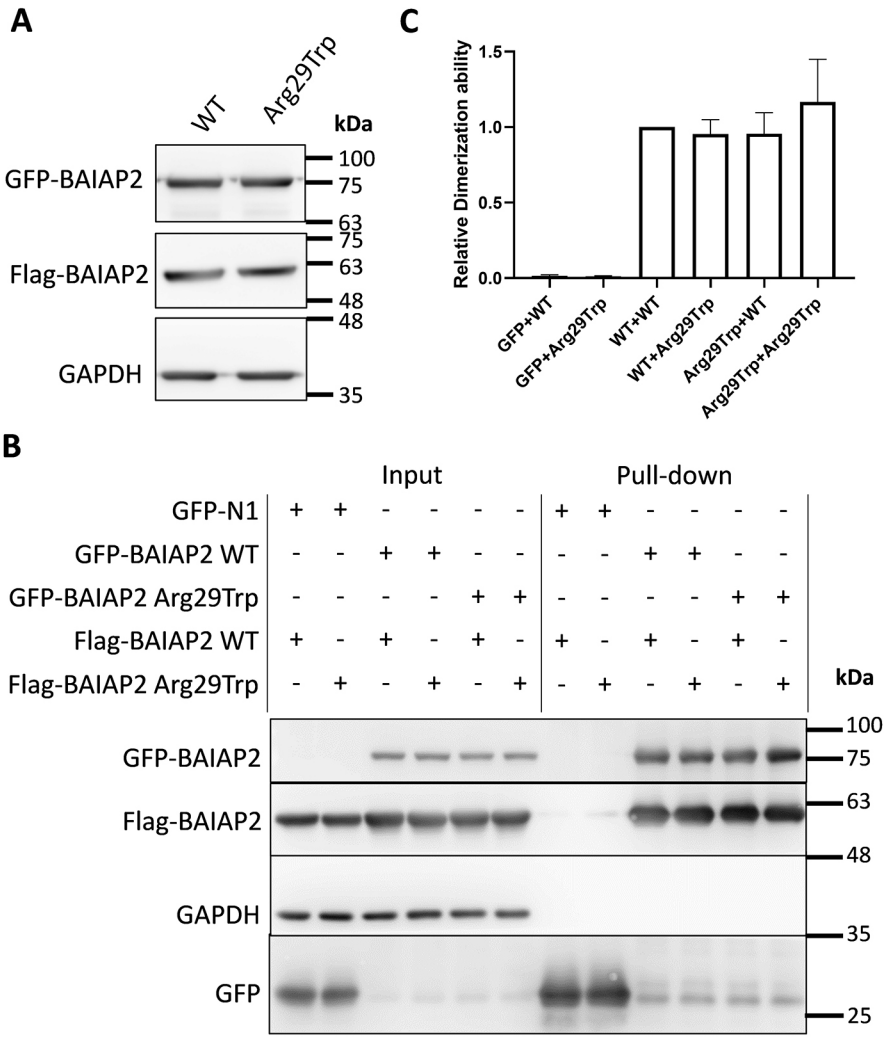

Fig. 6. Dimerization of WT BAIAP2 and the p.Arg29Trp variant using co-immunoprecipitation assay. (A) Expression of GFP-BAIAP2 and Flag-BAIAP2 in transfected HEK293T cells. (B) Co-immunoprecipitation of Flag-BAIAP2 with GFP-BAIAP2 using GFP pulldown assay. GFP-N1, GFP-BAIAP2 WT and GFP-BAIAP2 Arg29Trp were each co-transfected with Flag-BAIAP2 WT or Flag-BAIAP2 Arg29Trp into HEK293T cells. Protein complexes were then pulled down by GFP antibody. The amount of Flag-tagged BAIAP2 WT and Arg29Trp pulled down by GFP-tagged BAIAP2 were similar. (C) Bar graph showing dimerization ability relative to the BAIAP2 WT–WT interaction. The interaction of p.Arg29Trp with p.Arg29Trp was slightly increased, but there was no significant difference among all groups. Error bars represent s.e.m. $P>0.05$ (one-way ANOVA with post-hoc Tukey's test); $n=3$.

2017). Whether related mechanisms are involved in this phenotype requires future investigations.

Intriguingly, those cells arrested in the WM did not express the neuronal markers NeuN and Brn2 at P7, whereas most cells that reached layer II/III of the cortex were $NeuN^+$ and $Brn2^+$ (Fig. 4). The cells arrested in the WM also did not express the astrocyte and oligodendrocyte markers GFAP and Olig2 (Fig. S3). This observation suggested that the arrested cells may not determine their cell fate at this stage. Interestingly, fewer cells were arrested in the WM at P7 compared with E18.5 (Fig. 3B, Fig. S2). This suggests that neuronal migration may be delayed rather than blocked or that cells arrested in the WM degenerated progressively. What cell types they differentiate into or whether they survive at later developmental stages remains elusive. Furthermore, it is still unclear whether the abnormal cell fate was caused directly by BAIAP2 dysfunction in neuronal differentiation or an indirect effect of neuronal migration delay.

The precise mechanisms by which BAIAP2 mutation contributes to defects in neuronal morphogenesis and migration remain an interesting question. The newly identified p.Arg29Trp variant is located within the IMD (Fig. 1C), a region known for its ability to bind to the cell membrane and actin filaments (Yamagishi et al., 2004; Suetsugu et al., 2006; Mattila et al., 2007). Our investigations through immunofluorescence and cell fractionation studies showed that, indeed, BAIAP2 was mainly localized to the cell periphery (Fig. 7). The IMD, distinguished by its curved structure, induces outward cell membrane protrusions (Yamagishi et al., 2004; Suetsugu et al., 2006; Mattila et al., 2007). Upon activation through interactions with Cdc42 and the Rho GTPase family, BAIAP2 recruits its effector proteins, including WAVE2 (Wasf2), Mena (Enah), mDia2 (Diaph3), Eps8, SH2B1, Shank proteins and PSD95, to its C terminus. These proteins, in turn, employ BAIAP2 as an adaptor to orchestrate actin cytoskeleton organization and regulate membrane dynamics (Miki et al., 2000; Krugmann et al., 2001; Bockmann et al., 2002; Soltau et al., 2004; Disanza et al., 2006, 2013; Chen et al., 2015). Depending on different localizations and compositions, BAIAP2-based machinery is involved in various biological processes, such as filopodia formation, lamellipodia extension, and PSD complex assembly in neurons (Scita et al., 2008).

The *BAIAP2* gene undergoes multiple splicing events, yielding four isoforms (IRSp53 L-, M-, S- and T-forms) primarily distinguished by variations in their C termini (Scita et al., 2008). The S- and L-forms are predominantly expressed in the brain; they exhibit differences in the presence of a PDZ-binding motif in the S-form and a WH2 domain in the L-form. Our study reveals a transition from the L-form to T-form transition between E13.5 and E15.5 (Fig. 1D), potentially reflecting a functional shift from early neuronal development to synaptic formation. However, the roles of

Development (2024) 151, dev201912. doi:10.1242/dev.201912

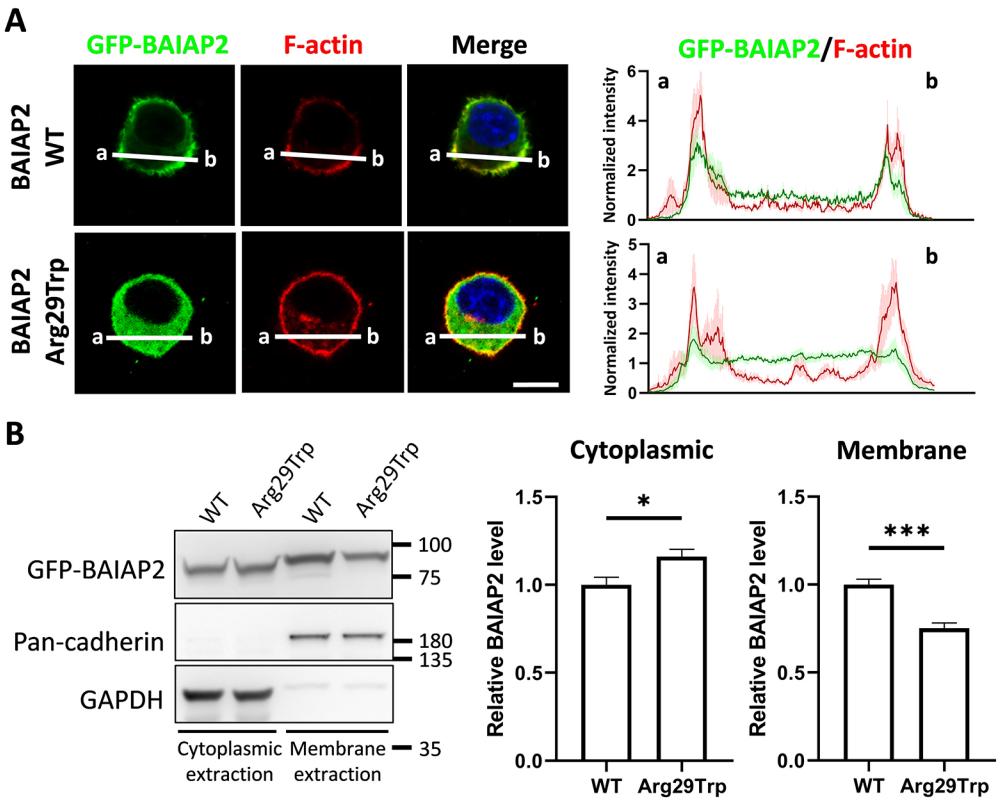

Fig. 7. The p.Arg29Trp variant interferes with BAIAP2 localization to the cell membrane. (A) The cellular localization of WT BAIAP2 and p.Arg29Trp (green) in transfected N2a cells. Cells were stained with phalloidin and DAPI to label actin filaments (red) and nuclei (blue), respectively. WT BAIAP2 was distributed to the cell margin, similar to the distribution of actin filaments. In contrast, the p.Arg29Trp variant dispersed its distribution to the cytoplasm. Scale bar: 10 µm. Intensity plots on the right show BAIAP2 (green) and actin filament (red) signals through the line crossing the cell in the left-hand panels. Green and pink shading represents the s.d. of the intensity among seven different cells. (B) WT BAIAP2 and p.Arg29Trp protein in the cytoplasmic and membrane fractions of transfected N2a cells. GAPDH and pan-cadherin were used as cytoplasmic and membrane markers. The bar graph shows BAIAP2 protein levels in cytoplasmic and membrane fractions relative to WT. The p.Arg29Trp variant is significantly increased in the cytoplasmic fraction and decreased in the membrane fraction. Error bars represent s.e.m. **P*<0.05, ****P*<0.001 (two-tailed unpaired *t*-test); *n*=6.

BAIAP2 in neuronal morphogenesis and migration remained relatively unexplored. Our observation that BAIAP2 dysfunction leads to more cells in the multipolar stage suggests a possible involvement of BAIAP2 in initiating and/or stabilizing the process designated as the leading process. Nevertheless, this hypothesis requires further detailed investigations. Moreover, we found that the p.Arg29Trp variant exhibited a diffuse cytoplasmic distribution, which could potentially affect actin architecture at the cell periphery. How this variant precisely affects actin binding and bundling, and downstream cellular functions remains an interesting

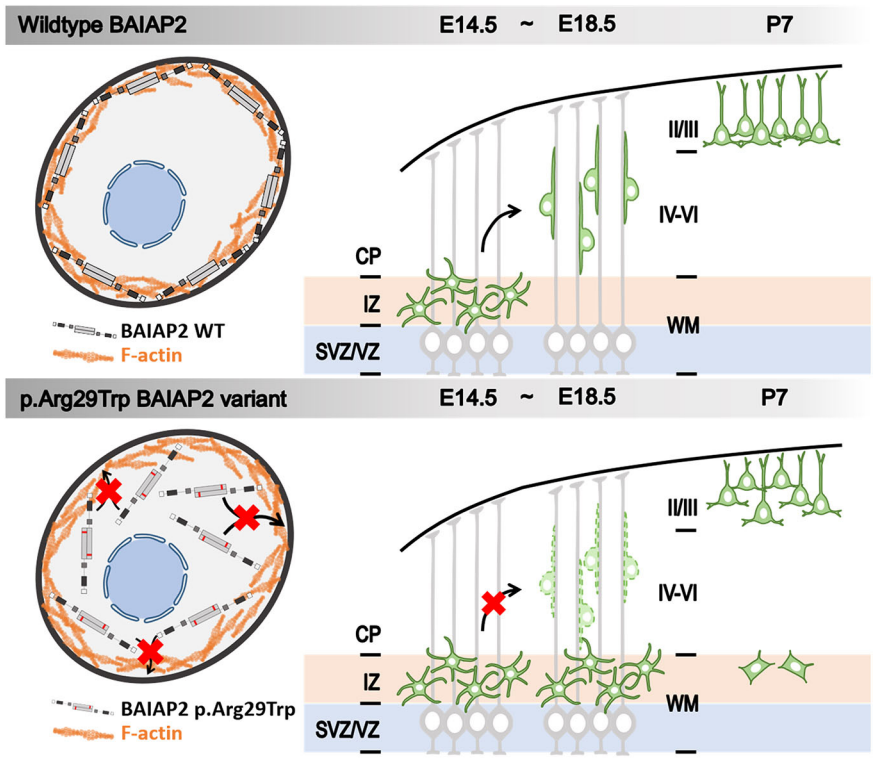

Fig. 8. Schematic of the possible pathogenic mechanism of the brain developmental defects caused by the p.Arg29Trp BAIAP2 variant. Under normal BAIAP2 expression (top), neurons transit from a multipolar to bipolar state and migrate to the CP in the developing mouse brain. In contrast, the p.Arg29Trp BAIAP2 variant (bottom) causes the arrest of neurons in the multipolar stage, which leads to neuronal migration delay. These effects may be caused by failure of the p.Arg29Trp variant to target the cell membrane.

Development (2024) 151, dev201912. doi:10.1242/dev.201912

area of investigation. Disruptions in these actin-related functions may, in part, account for the observed defects in morphogenesis and migration of developing neurons.

The loss-of-function observed/expected upper bound fraction (LOEUF) and predicted probability of haploinsufficiency (pHaplo) scores for *BAIAP2* stand at 0.429 and 0.73, respectively (Karczewski et al., 2020; Collins et al., 2022). These scores suggest that *BAIAP2* is a gene sensitive to dosage variations. Although our results from the mouse model did not show dominant-negative effects of the p.Arg29Trp variant on neuronal migration (Fig. S4), we cannot rule out such effects in human. There are still potential differences in BAIAP2 function between gyrencephalic and lissencephalic brains. Interestingly, *de novo* loss of copy number variation has also been reported in an individual with autism (Celestino-Soper et al., 2011). In addition, there were several pathogenic/likely pathogenic deletions that contain *BAIAP2* reported in the DECIPHER database (v11.18), and many of these individuals have microcephaly or lissencephaly. The genetic association of *BAIAP2* to a range of neurodevelopmental diseases implies that *BAIAP2* may play a broader role in the development and maintenance of normal neurological functions in the brain. Our finding of a novel *BAIAP2* variant causing lissencephaly further expands the clinical spectrum to more severe human neurodevelopmental disorders, suggesting multiple functional roles of BAIAP2 in different developmental stages of the brain.

MATERIALS AND METHODS

Ethics approval and consent to participate

The study was approved by the local human research ethics committee, and written consent was obtained from the parents. All experiments and animal maintenance were conducted according to protocols approved by the Institutional Animal Care and Use Committee (IACUC) at National Yang Ming Chiao Tung University.

Study subject

The proband and parents were referred to the genetic study program for lissencephaly at the Department of Neurology at Kaohsiung Chang Gung Memorial Hospital, Taiwan. Medical records and neuroimaging studies were reviewed by experienced pediatric neurologists and epileptologists. The study was approved by the local human research ethics committee, and written informed consent was obtained from the parents.

Whole-exome sequencing study

Trio whole-exome sequencing was performed as previously described (Tsai et al., 2017). Briefly, genome DNA was captured using IDT xGen Exome Research Panel V2 and sequenced using the Illumina NextSeq 2000 platform. Reads were mapped to the human reference sequence (hg19), and variants were called using the GATK variant caller. Because the majority of reported lissencephaly cases are *de novo* in origin and the parents in this family were unaffected, we focused on *de novo* variants. These variants were annotated using ANNOVAR and filtered to exclude those present in the Genome Aggregation Database (gnomAD), specifically targeting exonic/splicing variants that were not synonymous changes. Further prioritization of the remaining variants was based on the mechanism using VarElect (https://varelect.genecards.org/); genes encoding for proteins related to the cytoskeleton were selected.

Tissue processing and spatial transcriptome

Spatial transcriptome analysis (Visium, 10x Genomics) was performed on a brain sample from an embryonic C57BL/6 mouse at E15.5. The tissue processing followed the manufacturer's instructions. Briefly, fresh brain tissue was rapidly embedded in the Optimal Cutting Temperature (OCT) compound (Sakura Finetek) and frozen in an isopentane (Sigma-Aldrich) bath in liquid nitrogen. A cryostat (NX70; Thermo Fisher Scientific) was used to obtain 10-µm-thick sagittal brain sections, which were placed on pre-chilled Visium spatial tissue optimization (TO) slides or gene expression (GE) slides (10x Genomics). Histological images by Hematoxylin & Eosin staining were acquired using an inverted microscope IX83 (Olympus; 10× objective, NA=0.25). cDNA libraries were sequenced on a NovaSeq 6000 System (Illumina) with the NovaSeq S4 Reagent Kit (300 cycles). In our experiment, 1189 out of 5000 spots (23.8%) were covered by tissue, with an average of 191,168 reads and a medium of 3092 genes per spot. Initial processing of Visium data, including raw FASTQ files and images, was performed using Space Ranger software (version 1.2.1), and gene alignment utilized the mouse reference genome (MM10). Subsequent data analysis was carried out using Loupe Browser 6.4.0. The spatial gene transcriptome data is available at https://doi.org/10.57770/P3TK72Baiap2 expression was defined based on the $\log_2$-transformed rendering of unique molecular identifier counts in each spot. Violin plots were employed to display statistical values (maximum, minimum, mean and median) of *Baiap2* expression in each cluster.

In situ hybridization

The *Baiap2 in situ* hybridization probe sequence was amplified from mouse E15.5 developing cortex cDNA using the following primers: Baiap2_F: GGCCGCGGCCCCAACAAGATCCCAGACC; Baiap2_R: CCCGGGG-CGTGGGGACAGAGTGTCGATG. It was then cloned into a pGEM-T vector. The *Baiap2* antisense probe was prepared, and *in situ* hybridization was performed according to previously established methods (Hou et al., 2017). The signal was developed using the NBT/BCIP method, and images were acquired using a Zeiss Axioscan 7 Microscope Slide Scanner.

Human single-cell transcriptomics

The GW20 human embryonic cortex dataset was analyzed using Seurat v4.0 in RStudio. The number of principal components was determined using the ElbowPlot function, and 20 principal components were used to create uniform manifold approximation and projections (UMAPs) for human GW20. Gene expression data was computed and visualized using Seurat v4.0 and the Nebulosa R toolkit (Alquicira-Hernandez and Powell, 2021). Cells that displayed at least one read of *BAIAP2* mRNA were identified as *BAIAP2*-expressing cells.

shRNA and knockdown efficiency test

Mouse *Baiap2* shRNAs and scrambled controls were obtained from the RNAiCore of Academia Sinica. The oligo sequences of sh*Baiap2* were as follows: #54: 5′-CCGGCGGAAGTGACAGATTGCATATCTCGAGATA-TGCAATCTGTCACTTCCGTTTTTG-3′; #57: 5′-CGGCTATTTCGATG-CTCTGGTAAACTCGAGTTTACCAGAGCATCGAAATAGTTTTTG-3′; #312: 5′-CCGGTGATGCAACAGATGGCCAATACTCGAGTATTGGCC-ATCTGTTGCATCATTTTTG-3′; and #498: 5′-CCGGCATCGATGCCAT-CAGCAATAACTCGAGTTATTGCTGATGGCATCGATGTTTTTG-3′.

N2a cells were used to assess the knockdown efficiency of *Baiap2* shRNA. The shRNAs were transfected into N2a cells for 24 h, followed by incubation in 3 µg/ml puromycin for 48 h to select cells expressing sh*Baiap2*. Cell lysates were then collected for western blotting to compare BAIAP2 protein expression between groups.

BAIAP2 constructs

The WT pECE-M2-*BAIAP2*, with a flag tag on BAIAP2, was generously provided by Anne Brunet (Addgene plasmid #31656). The 85th nucleotide of *BAIAP2* was mutated from C to T using the Quikchange Lighting Site-Directed Mutagenesis Kit (210519-5, Agilent Technologies). The sequences of the forward and reverse primers for mutagenesis were 5′-CCCTAGCCTCTGGAACTTCAT-3′ and 5′-TGAAGTTCCAGAGGCTA-GGG-3′, respectively, with the mutation site underlined. Following mutagenesis, the products were transformed into XL10-Gold Ultracompetent cells (200315, Agilent Technologies) and amplified. The plasmids were finally extracted using the TOOLS Plasmid Mini kit (TT-A03-3, BioTools).

WT and mutant *BAIAP2* were cloned into pCAGIG and pEGFP-N1 (Clontech) vectors. pCAGIG was a gift from Connie Cepko (Addgene plasmid #11159) and was used in the animal experiment. pEGFP-N1-*BAIAP2* was used to observe cellular localization and for co-immunoprecipitation

Development (2024) 151, dev201912. doi:10.1242/dev.201912

experiments. Briefly, the *BAIAP2* sequence was amplified by PCR using Phusion High-Fidelity DNA Polymerase (M0530, New England Biolabs). When cloning *BAIAP2* to pCAGIG, the vector and insert were digested using EcoRV-HF (New England Biolabs) and NotI-HF (New England Biolabs), whereas EcoRI-HF (New England Biolabs) and BamHI-HF (New England Biolabs) were used for cloning into pEGFP-N1. Digested products were then ligated using T4 DNA Ligase (B0202, New England Biolabs) and transformed into JUMBO 80 High 108 HIT-DH5α competent cells (RH618-J80, HIT, Real Biotech). Transformed bacteria were incubated to amplify the DNA products, which were then extracted using the TOOLS Plasmid Mini kit (TT-A03-3, BioTools).

Cell culture and transfection

N2a cells (60026) were purchased from the Bioresource Collection and Research Centre (BCRC) in Taiwan and used for sh*Baiap2* knockdown efficiency testing, protein cellular localization, and protein subcellular fraction analysis. HEK293T cells (60019) were purchased from BCRC and used to assess protein expression and conduct co-immunoprecipitation. N2a and HEK293T cells were cultured in Dulbecco's Modified Eagle Medium supplemented with 10% L-glutamine, 10% penicillin-streptomycin (P/S), sodium pyruvate, sodium bicarbonate, and 10% fetal bovine serum. Transfection was carried out using a Lipofectamine 3000 kit (L3000075, Invitrogen) for 24 h to express target proteins.

Protein extraction and quantification

Mouse cortex tissue and cultured cells were lysed in RIPA buffer (SLBT1336, Sigma-Aldrich) supplemented with 10% PhosSTOP (Roche Biochemical) and 10% protease inhibitor (Roche Biochemical Reagents). The lysates were then centrifuged at 15,000 ***g*** for 15 min to separate cellular debris. Protein concentrations were determined using the Pierce BCA Protein Assay Kit (23225, Thermo Fisher Scientific).

Western blotting

Protein samples were mixed with 5× loading dye [250 mM pH 6.8 Tris-HCl, 10% sodium dodecyl sulfate (SDS), 30% glycerol, 5% β-mercaptoethanol and 0.02% Bromophenol Blue] and boiled at 100°C for 10 min before electrophoresis on SDS-PAGE gels. Proteins were separated based on molecular weight and then transferred to polyvinylidene difluoride membranes (R1NB68664, Merck Millipore). Following blocking with 5% milk in 0.1% TTBS (0.1% Tween-20 in TBS buffer) for 1 h, primary antibodies were applied to blot proteins at 4°C overnight, followed by a 2-h incubation with horseradish peroxidase (HRP)-conjugated secondary antibodies at room temperature (Ibrahim et al., 2020).

Primary antibodies included rabbit polyclonal antibody against BAIAP2 (1:200; GTX115421, GeneTex), chicken polyclonal antibody against GFP (1:7500; ab13970, Abcam), mouse monoclonal antibody against Flag tag (1:2000; 66008-2-Ig, Proteintech), rabbit monoclonal antibody against pan-cadherin (1:2000; GTX61612, GeneTex) and mouse monoclonal antibody against GAPDH (1:10,000; 60004-1-lg, Proteintech). Secondary antibodies were HRP-conjugated goat antibodies against rabbit (#12-349, Sigma-Aldrich), mouse (AP124P, Merck Millipore) and chicken (ab205721, Abcam).

After immunostaining, Immobilon Western Chemiluminescent HRP Substrate (WBKLS0500, Merck Millipore) was applied to the membrane to react with HRP and emit luminescence. Luminescence was detected using a Fujifilm LAS-4000 gel imager to generate the images, which were then analyzed using ImageJ.

Co-immunoprecipitation

GFP-BAIAP2 and flag-BAIAP2 were co-transfected into HEK293T cells to form BAIAP2 dimers. An empty vector, pEGFP-N1, served as the negative control for co-immunoprecipitation. After protein extraction and quantification, the proteins were incubated with GFP-Trap Magnetic Agarose (gtma-20, ChromoTek) at 4°C overnight. The beads separated GFP or GFP-BAIAP2 and their binding partners from the extract and were boiled in 1× loading dye. Both co-immunoprecipitated protein and 10% input proteins were used for western blotting, with GAPDH as the internal control for input proteins.

Fractionation

HEK293T cells were transfected to express WT BAIAP2 and the p.Arg29Trp (R29W) variant. After cell collection, subcellular fractions were obtained using the Subcellular Protein Fractionation Kit for Cultured Cells (78840, Thermo Fisher Scientific). Protein expression in cytoplasmic and membrane fractions was analyzed by western blotting, with GAPDH and pan-cadherin serving as internal standards of cytoplasmic and membrane fractions, respectively.

IUE

Pregnant ICR mice (BioLASCO) with E14.5 embryos were subjected to surgery. Following anesthetization with isoflurane, the uterine horns were exposed. Constructs with US2-GFP in EB buffer (TT-A03-3, BioTools) containing 2.5 mg/ml Fast Green (Sigma-Aldrich) were then injected into the lateral ventricle of embryos through the uterine wall. Electroporation was performed using 5 mm Tweezertrodes (45-0489, Harvard Apparatus), delivering five 40 V electric pulses for 50 ms with 450 ms intervals. The concentration of construct electroporated into mouse embryos varied according to different experiments. To explore the effects of knocking down *Baiap2* on cortical development, shCtrls (TRC1 and TRC2) and sh*Baiap2* were used at a concentration of 1.5 µg/µl. To investigate the effects of overexpressing *BAIAP2* in cortical development, the vector (pCAGIG), WT and p.Arg29Trp *BAIAP2* were electroporated at 0.25 µg/µl. To identify the ability of BAIAP2 to rescue the phenotype of sh*Baiap2*, sh*Baiap2* was electroporated at 0.75 µg/µl and *BAIAP2* at 0.5 µg/µl. The US2-GFP construct was a generous gift from Dr Jenn-Ya Yu, National Yang Ming Chiao Tung University, Taiwan. After IUE, the uterine horns were repositioned in the abdominal cavity, and the abdominal incision was closed.

After designated days post IUE, embryos or infant mice were perfused with PBS and 4% paraformaldehyde (PFA) in PBS. Brains were then collected, fixed in 4% PFA at 4°C overnight, and embedded in 4% low-melting agarose (AMRESCO). The embedded brains were sectioned into 100-µm-thick slices using a Leica VT1000S vibrating microtome and prepared for immunofluorescence staining. For endogenous BAIAP2 immunofluorescence staining, brains embedded in Tissue-Tek® O.C.T. Compound (Sakura Finetek) were sectioned into 12-µm-thick slices using a Thermo CryoStar NX70 cryostat (Thermo Fisher Scientific).

Immunofluorescence staining

For vibratome-sectioned brain slice staining, samples were incubated in blocking buffer [5% bovine serum albumin (BSA), 10% normal goat serum (NGS) in PBS with 0.2% Triton X-100 (PBST)] for 1 h at room temperature. Following blocking, brain sections were incubated in primary antibodies in 0.2% PBST containing 5% BSA and 5% NGS for two nights at 4°C, followed by three PBS washes and incubation with secondary antibodies for 2 h at room temperature. Finally, brain sections were stained with DAPI to label nuclei for 1.5 h at room temperature.

For endogenous BAIAP2 immunofluorescence staining, cryostat-sectioned samples were incubated in blocking buffer (10% NGS in PBS with 0.1% PBST and 0.2% Tween 20) for 1 h at room temperature. Following blocking, brain sections were incubated in primary antibodies in blocking buffer diluted 1:10 overnight at 4°C, followed by three PBS washes and incubation with secondary antibodies for 2 h at room temperature. Finally, brain sections were stained with DAPI to label nuclei for 15 min at room temperature.

Primary antibodies used for brain slice staining were: rabbit polyclonal antibody against BAIAP2 (1:200; HPA023310, Sigma-Aldrich), rabbit polyclonal antibody against NeuN (1:500; ABN78, Merck Millipore), mouse monoclonal antibody against Brn2 (1:500; sc-393324, Santa Cruz Biotechnology), rabbit polyclonal antibody against GFAP (1:500; Z0334, Dako), rabbit polyclonal antibody against Olig2 (1:500; NBP1-28667, Novus Biologicals) and rabbit polyclonal antibody against HA (1:500; GTX115044, GeneTex). Alexa Fluor 546-conjugated goat antibodies against mouse and rabbit IgG (2335720 and 2423676, Thermo Fisher Scientific) were used as secondary antibodies.

For cultured cell staining, glass slides with attached cells were fixed in 4% PFA on ice for 20 min and permeabilized in 0.1% PBST on ice for 8 min.

Slides were then blocked in PBS with 0.05% sodium azide (Sigma-Aldrich), 5% NGS and 5% BSA for 1 h of shaking at room temperature. Slides were incubated in primary antibodies with blocking buffer at 4°C overnight, followed by 2 h of incubation with secondary antibodies and 15 min of DAPI staining at room temperature (Hsiao et al., 2018; Nian et al., 2019; Tsai et al., 2019).

The primary antibody used for cultured cell staining was mouse monoclonal antibody against GFP (1:1000; ab1218, Abcam), and the secondary antibody was Alexa Fluor 488-conjugated goat anti-mouse IgG (2220848, Thermo Fisher Scientific). In addition, Alexa Fluor 546-conjugated phalloidin (A22283, Thermo Fisher Scientific) was used to label actin filaments in cells.

Confocal microscopy

Following immunostaining, images were collected and processed using a Zeiss LSM 700 confocal microscope and ZEN software (Zeiss). Stained cells were imaged at 100× magnification using an oil lens, and the brain slices were imaged at 20× magnification using an air lens. Image analysis was performed using ImageJ. *z*-series images were acquired at 1-µm intervals, and a projection of each stack was utilized for generating figures. The images were subjected to contrast adjustment, assembly into montages, and pseudocolor application using ZEN. In IUE experiments, each brain slice contained 300-600 GFP-positive cells in the neocortex; all the cells were included in the statistical analysis. At least three slices per animal were used for quantification. Cell counting in brain slices was conducted using the 'Cell Counter' plugin in ImageJ, with careful inspection. For experiments involving co-labeling or cell/process counting, images from individual optical sections were carefully examined.

Statistics

For comparisons between two groups, unpaired two-tailed *t*-test was applied. In cases involving more than two groups, one-way ANOVA was applied, with post-hoc Tukey's multiple comparison tests. Statistical analysis was conducted using GraphPad Prism software. Statistical data are presented as mean±s.e.m., and significance levels are indicated by asterisks (*P<0.05, **P<0.01,***P<0.001, ****P<0.0001).

Acknowledgements

We express our gratitude to the individual with lissencephaly used in this study as well as their family, individuals used as controls, and referring doctors for participating in this study. We also thank the Genomic and Proteomic Core Laboratory, Kaohsiung Chang Gung Memorial Hospital, for technical support with whole exome sequencing. We acknowledge the cDNA library construction and the analysis of spatial transcriptome provided by the Genomics Center for Clinical and Biotechnological Applications of the National Core Facility for Biopharmaceuticals, Taiwan (NSTC 112-2740-B-A49-001). The National Core Facility for Biopharmaceuticals (NCFB) and the National Science and Technology Council provided computational and storage resources.

Competing interests

The authors declare no competing or financial interests.

Author contributions

Conceptualization: M.-H.T., W.-C.L., J.-W.T.; Methodology: W.-C.L., F.-S.N., H.-Y.C., H.-J.Z., S.-S.H., C.-H.H., P.-S.H., C.-Y.T.; Validation: M.-H.T., W.-C.L., S.-Y.C., F.-S.N., H.-Y.C., H.-J.Z.; Formal analysis: M.-H.T., W.-C.L., M.-Y.H., C.-H.H., C.-Y.T., M.-H.L.; Investigation: M.-H.T., W.-C.L., S.-Y.C., M.-Y.H., F.-S.N., H.-Y.C., H.-J.Z., S.-S.H., C.-Y.T.; Data curation: W.-C.L., M.-H.L.; Writing - original draft: M.-H.T., W.-C.L., P.-S.H., J.-W.T.; Writing - review & editing: M.-H.T., W.-C.L., S.-Y.C., M.-Y.H., F.-S.N., H.-Y.C., H.-J.Z., S.-S.H., C.-H.H., P.-S.H., C.-Y.T., M.-H.L., J.-W.T.; Visualization: W.-C.L., F.-S.N.; Supervision: M.-H.T., P.-S.H., J.-W.T.; Funding acquisition: M.-H.T., M.-H.L., J.-W.T.

Funding

This study was supported by grants from the National Science and Technology Council, Taiwan (108-2638-B-010-001-MY2, 108-2321-B-010-011-MY2, 110-2628-B-A49A-506, 111-2628-B-A49-016, 112-2628-B-A49-005 and 112-2314-B-A49-075 to J.-W.T.; 110-2314-B-182-057-MY3 and 110-2314-B-182A-076-MY3 to M.-H.T.), the National Health Research Institutes (NHRI-EX109-10904NI to J.-W.T.; NHRI-EX111-11022NI to M.-H.T.), the Brain Research Center, National Yang-Ming University through the Featured Areas Research Center Program within the framework of the Higher Education Sprout Project by the Ministry of Education (MOE), Taiwan (J.-W.T.), and the Chang Gung Medical Foundation (CMRP8L1331, CMRPG8M1091 and CIRPG8M0091 to M.-H.T.).

Data availability

The spatial gene transcriptome data are available at https://doi.org/10.57770/P3TK72

The people behind the papers

This article has an associated 'The people behind the papers' interview with some of the authors.

Peer review history

The peer review history is available online at https://journals.biologists.com/dev/lookup/doi/10.1242/dev.201912.reviewer-comments.pdf

References

Allanson, J. E., Ledbetter, D. H. and Dobyns, W. B. (1998). Classical lissencephaly syndromes: does the face reflect the brain? *J. Med. Genet.* **35**, 920-923. doi:10.1136/jmg.35.11.920

Alquicira-Hernandez, J. and Powell, J. E. (2021). Nebulosa recovers single-cell gene expression signals by kernel density estimation. *Bioinformatics* **37**, 2485-2487. doi:10.1093/bioinformatics/btab003

Barkovich, A. J., Koch, T. K. and Carrol, C. L. (1991). The spectrum of lissencephaly: report of ten patients analyzed by magnetic resonance imaging. *Ann. Neurol.* **30**, 139-146. doi:10.1002/ana.410300204

Bhaduri, A., Sandoval-Espinosa, C., Otero-Garcia, M., Oh, I., Yin, R., Eze, U. C., Nowakowski, T. J. and Kriegstein, A. R. (2021). An atlas of cortical arealization identifies dynamic molecular signatures. *Nature* **598**, 200-204. doi:10.1038/s41586-021-03910-8

Bockmann, J., Kreutz, M. R., Gundelfinger, E. D. and Böckers, T. M. (2002). ProSAP/Shank postsynaptic density proteins interact with insulin receptor tyrosine kinase substrate IRSp53. *J. Neurochem.* **83**, 1013-1017. doi:10.1046/j.1471-4159.2002.01204.x

Celestino-Soper, P. B., Shaw, C. A., Sanders, S. J., Li, J., Murtha, M. T., Ercan-Sencicek, A. G., Davis, L., Thomson, S., Gambin, T., Chinault, A. C. et al. (2011). Use of array CGH to detect exonic copy number variants throughout the genome in autism families detects a novel deletion in TMLHE. *Hum. Mol. Genet.* **20**, 4360-4370. doi:10.1093/hmg/ddr363

Chang, H. Y., Cheng, H. Y., Tsao, A. N., Liu, C. and Tsai, J. W. (2019). Multiple functions of KBP in neural development underlie brain anomalies in Goldberg-Shprintzen syndrome. *Front. Mol. Neurosci.* **12**, 265. doi:10.3389/fnmol.2019.00265

Chen, K. W., Chang, Y. J. and Chen, L. (2015). SH2B1 orchestrates signaling events to filopodium formation during neurite outgrowth. *Commun. Integr. Biol.* **8**, e1044189. doi:10.1080/19420889.2015.1044189

Chen, J. L., Chang, C. H. and Tsai, J. W. (2019). Gli2 Rescues delays in brain development induced by Kif3a dysfunction. *Cereb. Cortex* **29**, 751-764. doi:10.1093/cercor/bhx356

Chen, A., Liao, S., Cheng, M., Ma, K., Wu, L., Lai, Y., Qiu, X., Yang, J., Xu, J., Hao, S. et al. (2022). Spatiotemporal transcriptomic atlas of mouse organogenesis using DNA nanoball-patterned arrays. *Cell* **185**, 1777-1792.e21. doi:10.1016/j.cell.2022.04.003

Chen, Y. A., Lu, I. L. and Tsai, J. W. (2018). Contactin-1/F3 regulates neuronal migration and morphogenesis through modulating RhoA activity. *Front. Mol. Neurosci.* **11**, 422. doi:10.3389/fnmol.2018.00422

Choi, J., Ko, J., Racz, B., Burette, A., Lee, J. R., Kim, S., Na, M., Lee, H. W., Kim, K., Weinberg, R. J. et al. (2005). Regulation of dendritic spine morphogenesis by insulin receptor substrate 53, a downstream effector of Rac1 and Cdc42 small GTPases. *J. Neurosci.* **25**, 869-879. doi:10.1523/JNEUROSCI.3212-04.2005

Collins, R. L., Glessner, J. T., Porcu, E., Lepamets, M., Brandon, R., Lauricella, C., Han, L., Morley, T., Niestroj, L. M., Ulirsch, J. et al. (2022). A cross-disorder dosage sensitivity map of the human genome. *Cell* **185**, 3041-3055.e25. doi:10.1016/j.cell.2022.06.036

des Portes, V., Francis, F., Pinard, J. M., Desguerre, I., Moutard, M. L., Snoeck, I., Meiners, L. C., Capron, F., Cusmai, R., Ricci, S. et al. (1998). doublecortin is the major gene causing X-linked subcortical laminar heterotopia (SCLH). *Hum. Mol. Genet.* **7**, 1063-1070. doi:10.1093/hmg/7.7.1063

Di Donato, N., Timms, A. E., Aldinger, K. A., Mirzaa, G. M., Bennett, J. T., Collins, S., Olds, C., Mei, D., Chiari, S., Carvill, G. et al. (2018). Analysis of 17 genes detects mutations in 81% of 811 patients with lissencephaly. *Genet. Med.* **20**, 1354-1364. doi:10.1038/gim.2018.8

Disanza, A., Bisi, S., Winterhoff, M., Milanesi, F., Ushakov, D. S., Kast, D., Marighetti, P., Romet-Lemonne, G., Müller, H. M., Nickel, W. et al. (2013). CDC42 switches IRSp53 from inhibition of actin growth to elongation by clustering of VASP. *EMBO J.* **32**, 2735-2750. doi:10.1038/emboj.2013.208

Disanza, A., Mantoani, S., Hertzog, M., Gerboth, S., Frittoli, E., Steffen, A., Berhoerster, K., Kreienkamp, H. J., Milanesi, F., Di Fiore, P. P. et al. (2006).

Regulation of cell shape by Cdc42 is mediated by the synergic actin-bundling activity of the Eps8-IRSp53 complex. *Nat. Cell Biol.* **8**, 1337-1347. doi:10.1038/ncb1502

Dobyns, W. B. (2010). The clinical patterns and molecular genetics of lissencephaly and subcortical band heterotopia. *Epilepsia* **51** Suppl. 1, 5-9. doi:10.1111/j.1528-1167.2009.02433.x

Dobyns, W. B. and Truwit, C. L. (1995). Lissencephaly and other malformations of cortical development: 1995 update. *Neuropediatrics* **26**, 132-147. doi:10.1055/s-2007-979744

Dosemeci, A., Burch, A., Loo, H., Toy, D. and Tao-Cheng, J. H. (2017). IRSp53 accumulates at the postsynaptic density under excitatory conditions. *PLoS One* **12**, e0190250. doi:10.1371/journal.pone.0190250

Fry, A. E., Cushion, T. D. and Pilz, D. T. (2014). The genetics of lissencephaly. *Am. J. Med. Genet. C Semin. Med. Genet.* **166c**, 198-210. doi:10.1002/ajmg.c.31402

Gleeson, J. G., Allen, K. M., Fox, J. W., Lamperti, E. D., Berkovic, S., Scheffer, I., Cooper, E. C., Dobyns, W. B., Minnerath, S. R., Ross, M. E. et al. (1998). Doublecortin, a brain-specific gene mutated in human X-linked lissencephaly and double cortex syndrome, encodes a putative signaling protein. *Cell* **92**, 63-72. doi:10.1016/S0092-8674(00)80899-5

Gleeson, J. G., Lin, P. T., Flanagan, L. A. and Walsh, C. A. (1999). Doublecortin is a microtubule-associated protein and is expressed widely by migrating neurons. *Neuron* **23**, 257-271. doi:10.1016/S0896-6273(00)80778-3

Hong, S. E., Shugart, Y. Y., Huang, D. T., Shahwan, S. A., Grant, P. E., Hourihane, J. O., Martin, N. D. and Walsh, C. A. (2000). Autosomal recessive lissencephaly with cerebellar hypoplasia is associated with human RELN mutations. *Nat. Genet.* **26**, 93-96. doi:10.1038/79246

Hou, P. S., Kumamoto, T. and Hanashima, C. (2017). A sensitive and versatile in situ hybridization protocol for gene expression analysis in developing amniote brains. *Methods Mol. Biol.* **1650**, 319-334. doi:10.1007/978-1-4939-7216-6_22

Hsiao, C. J., Chang, C. H., Ibrahim, R. B., Lin, I. H., Wang, C. H., Wang, W. J. and Tsai, J. W. (2018). Gli2 modulates cell cycle re-entry through autophagy-mediated regulation of the length of primary cilia. *J. Cell Sci.* **131**, jcs221218. doi:10.1242/jcs.221218

Ibrahim, R. B., Yeh, S. Y., Lin, K. P., Ricardo, F., Yu, T. Y., Chan, C. C., Tsai, J. W. and Liu, Y. T. (2020). Cellular secretion and cytotoxicity of transthyretin mutant proteins underlie late-onset amyloidosis and neurodegeneration. *Cell. Mol. Life Sci.* **77**, 1421-1434. doi:10.1007/s00018-019-03357-1

Jheng, G. W., Hur, S. S., Chang, C. M., Wu, C. C., Cheng, J. S., Lee, H. H., Chung, B. C., Wang, Y. K., Lin, K. H., Del Álamo, J. C. et al. (2018). Lis1 dysfunction leads to traction force reduction and cytoskeletal disorganization during cell migration. *Biochem. Biophys. Res. Commun.* **497**, 869-875. doi:10.1016/j.bbrc.2018.02.151

Karczewski, K. J., Francioli, L. C., Tiao, G., Cummings, B. B., Alföldi, J., Wang, Q., Collins, R. L., Laricchia, K. M., Ganna, A., Birnbaum, D. P. et al. (2020). The mutational constraint spectrum quantified from variation in 141,456 humans. *Nature* **581**, 434-443. doi:10.1038/s41586-020-2308-7

Keays, D. A., Tian, G., Poirier, K., Huang, G. J., Siebold, C., Cleak, J., Oliver, P. L., Fray, M., Harvey, R. J., Molnár, Z. et al. (2007). Mutations in alpha-tubulin cause abnormal neuronal migration in mice and lissencephaly in humans. *Cell* **128**, 45-57. doi:10.1016/j.cell.2006.12.017

Kitamura, K., Yanazawa, M., Sugiyama, N., Miura, H., Iizuka-Kogo, A., Kusaka, M., Omichi, K., Suzuki, R., Kato-Fukui, Y., Kamiirisa, K. et al. (2002). Mutation of ARX causes abnormal development of forebrain and testes in mice and X-linked lissencephaly with abnormal genitalia in humans. *Nat. Genet.* **32**, 359-369. doi:10.1038/ng1009

Kriegstein, A. R. and Noctor, S. C. (2004). Patterns of neuronal migration in the embryonic cortex. *Trends Neurosci.* **27**, 392-399. doi:10.1016/j.tins.2004.05.001

Krugmann, S., Jordens, I., Gevaert, K., Driessens, M., Vandekerckhove, J. and Hall, A. (2001). Cdc42 induces filopodia by promoting the formation of an IRSp53: Mena complex. *Curr. Biol.* **11**, 1645-1655. doi:10.1016/S0960-9822(01)00506-1

Lin, J. R., Cheng, J. F., Liu, Y. T., Hsu, T. R., Lin, K. M., Chen, C., Lin, C. L., Tsai, M. H. and Tsai, J. W. (2022). Novel lissencephaly-associated DCX variants in the C-terminal DCX domain affect microtubule binding and dynamics. *Epilepsia* **63**, 1253-1265. doi:10.1111/epi.17198

Lo Nigro, C., Chong, C. S., Smith, A. C., Dobyns, W. B., Carrozzo, R. and Ledbetter, D. H. (1997). Point mutations and an intragenic deletion in LIS1, the lissencephaly causative gene in isolated lissencephaly sequence and Miller-Dieker syndrome. *Hum. Mol. Genet.* **6**, 157-164. doi:10.1093/hmg/6.2.157

Lu, I. L., Chen, C., Tung, C. Y., Chen, H. H., Pan, J. P., Chang, C. H., Cheng, J. S., Chen, Y. A., Wang, C. H., Huang, C. W. et al. (2018). Identification of genes associated with cortical malformation using a transposon-mediated somatic mutagenesis screen in mice. *Nat. Commun.* **9**, 2498. doi:10.1038/s41467-018-04880-8

Mattila, P. K., Pykäläinen, A., Saarikangas, J., Paavilainen, V. O., Vihinen, H., Jokitalo, E. and Lappalainen, P. (2007). Missing-in-metastasis and IRSp53 deform PI(4,5)P2-rich membranes by an inverse BAR domain-like mechanism. *J. Cell Biol.* **176**, 953-964. doi:10.1083/jcb.200609176

Miki, H., Yamaguchi, H., Suetsugu, S. and Takenawa, T. (2000). IRSp53 is an essential intermediate between Rac and WAVE in the regulation of membrane ruffling. *Nature* **408**, 732-735. doi:10.1038/35047107

Nian, F. S., Li, L. L., Cheng, C. Y., Wu, P. C., Lin, Y. T., Tang, C. Y., Ren, B. S., Tai, C. Y., Fann, M. J., Kao, L. S. et al. (2019). Rab18 collaborates with Rab7 to modulate lysosomal and autophagy activities in the nervous system: an overlapping mechanism for warburg micro syndrome and Charcot-Marie-tooth neuropathy type 2B. *Mol. Neurobiol.* **56**, 6095-6105. doi:10.1007/s12035-019-1471-z

Oda, K., Shiratsuchi, T., Nishimori, H., Inazawa, J., Yoshikawa, H., Taketani, Y., Nakamura, Y. and Tokino, T. (1999). Identification of BAIAP2 (BAI-associated protein 2), a novel human homologue of hamster IRSp53, whose SH3 domain interacts with the cytoplasmic domain of BAI1. *Cytogenet. Cell Genet.* **84**, 75-82. doi:10.1159/000015219

Reiner, O., Carrozzo, R., Shen, Y., Wehnert, M., Faustinella, F., Dobyns, W. B., Caskey, C. T. and Ledbetter, D. H. (1993). Isolation of a Miller-Dieker lissencephaly gene containing G protein beta-subunit-like repeats. *Nature* **364**, 717-721. doi:10.1038/364717a0

Santana, J. and Marzolo, M. P. (2017). The functions of Reelin in membrane trafficking and cytoskeletal dynamics: implications for neuronal migration, polarization and differentiation. *Biochem. J.* **474**, 3137-3165. doi:10.1042/BCJ20160628

Scita, G., Confalonieri, S., Lappalainen, P. and Suetsugu, S. (2008). IRSp53: crossing the road of membrane and actin dynamics in the formation of membrane protrusions. *Trends Cell Biol.* **18**, 52-60. doi:10.1016/j.tcb.2007.12.002

Soltau, M., Berhörster, K., Kindler, S., Buck, F., Richter, D. and Kreienkamp, H. J. (2004). Insulin receptor substrate of 53 kDa links postsynaptic shank to PSD-95. *J. Neurochem.* **90**, 659-665. doi:10.1111/j.1471-4159.2004.02523.x

Suetsugu, S., Murayama, K., Sakamoto, A., Hanawa-Suetsugu, K., Seto, A., Oikawa, T., Mishima, C., Shirouzu, M., Takenawa, T. and Yokoyama, S. (2006). The RAC binding domain/IRSp53-MIM homology domain of IRSp53 induces RAC-dependent membrane deformation. *J. Biol. Chem.* **281**, 35347-35358. doi:10.1074/jbc.M606814200

Tsai, J. W., Chen, Y., Kriegstein, A. R. and Vallee, R. B. (2005). LIS1 RNA interference blocks neural stem cell division, morphogenesis, and motility at multiple stages. *J. Cell Biol.* **170**, 935-945. doi:10.1083/jcb.200505166

Tsai, M. H., Kuo, P. W., Myers, C. T., Li, S. W., Lin, W. C., Fu, T. Y., Chang, H. Y., Mefford, H. C., Chang, Y. C. and Tsai, J. W. (2016). A novel DCX missense mutation in a family with X-linked lissencephaly and subcortical band heterotopia syndrome inherited from a low-level somatic mosaic mother: Genetic and functional studies. *Eur. J. Paediatr. Neurol.* **20**, 788-794. doi:10.1016/j.ejpn.2016.05.010

Tsai, M. H., Chan, C. K., Chang, Y. C., Yu, Y. T., Chuang, S. T., Fan, W. L., Li, S. C., Fu, T. Y., Chang, W. N., Liou, C. W. et al. (2017). DEPDC5 mutations in familial and sporadic focal epilepsy. *Clin. Genet.* **92**, 397-404. doi:10.1111/cge.12992

Tsai, M. H., Nian, F. S., Hsu, M. H., Liu, W. S., Liu, Y. T., Liu, C., Lin, P. H., Hwang, D. Y., Chuang, Y. C. and Tsai, J. W. (2019). PRRT2 missense mutations cluster near C-terminus and frequently lead to protein mislocalization. *Epilepsia* **60**, 807-817. doi:10.1111/epi.14725

Tsai, M. H., Cheng, H. Y., Nian, F. S., Liu, C., Chao, N. H., Chiang, K. L., Chen, S. F. and Tsai, J. W. (2020a). Impairment in dynein-mediated nuclear translocation by BICD2 C-terminal truncation leads to neuronal migration defect and human brain malformation. *Acta Neuropathol. Commun.* **8**, 106. doi:10.1186/s40478-020-00971-0

Tsai, M. H., Muir, A. M., Wang, W. J., Kang, Y. N., Yang, K. C., Chao, N. H., Wu, M. F., Chang, Y. C., Porter, B. E., Jansen, L. A. et al. (2020b). Pathogenic Variants in CEP85L Cause Sporadic and Familial Posterior Predominant Lissencephaly. *Neuron* **106**, 237-245.e8. doi:10.1016/j.neuron.2020.01.027

Yamagishi, A., Masuda, M., Ohki, T., Onishi, H. and Mochizuki, N. (2004). A novel actin bundling/filopodium-forming domain conserved in insulin receptor tyrosine kinase substrate p53 and missing in metastasis protein. *J. Biol. Chem.* **279**, 14929-14936. doi:10.1074/jbc.M309408200